IJMMM International Journal of Minerals, Metallurgy and Materials 矿物冶金与材料学报（英文版）

Influence of manganese on vanadium precipitation and V_2O_5 purity based on different roasting methods of vanadium slag

Lan Zhang, Tao Jiang, Jing Wen, Tangxia Yu, Changqing Li, and Xinyu An

Cite this article as:
Lan Zhang, Tao Jiang, Jing Wen, Tangxia Yu, Changqing Li, and Xinyu An, Influence of manganese on vanadium precipitation and V_2O_5 purity based on different roasting methods of vanadium slag, *Int. J. Miner. Metall. Mater.*, 33(2026), No. 2, pp. 531-544. https://doi.org/10.1007/s12613-025-3192-9

View the article online at SpringerLink or IJMMM Webpage.

Articles you may be interested in

Zhengpei Yan, Shili Zheng, and Yang Zhang, Effects of vanadium valences on the solubility in Fe_2TiO_5 for helping to understand calcification roasting of vanadium slag, *Int. J. Miner. Metall. Mater.*, 32(2025), No. 12, pp. 2920-2929. https://doi.org/10.1007/s12613-025-3184-9

Tangxia Yu, Tao Jiang, Jing Wen, Hongyan Sun, Ming Li, and Yi Peng, Effect of chemical composition on the element distribution, phase composition and calcification roasting process of vanadium slag, *Int. J. Miner. Metall. Mater.*, 29(2022), No. 12, pp. 2144-2151. https://doi.org/10.1007/s12613-021-2334-y

Junjie Shi, Yumo Zhai, Yuchao Qiu, Changle Hou, Jingjing Dong, Maoxi Yao, Haolun Li, Yongrong Zhou, and Jianzhong Li, Phase equilibria relations in the V_2O_5-rich part of the Fe_2O_3–TiO_2–V_2O_5 system at 1200°C related to converter vanadium-bearing slag, *Int. J. Miner. Metall. Mater.*, 31(2024), No. 9, pp. 2017-2024. https://doi.org/10.1007/s12613-024-2845-4

Yun Guo, Hong-yi Li, Yi-heng Yuan, Jie Huang, Jiang Diao, Gang Li, and Bing Xie, Microemulsion leaching of vanadium from sodium-roasted vanadium slag by fusion of leaching and extraction processes, *Int. J. Miner. Metall. Mater.*, 28(2021), No. 6, pp. 974-980. https://doi.org/10.1007/s12613-020-2105-1

Jing Wen, Hongyan Sun, Tao Jiang, Bojian Chen, Fangfang Li, and Mengxia Liu, Comparison of the interface reaction behaviors of CaO–V_2O_5 and MnO_2–V_2O_5 solid-state systems based on the diffusion couple method, *Int. J. Miner. Metall. Mater.*, 30(2023), No. 5, pp. 834-843. https://doi.org/10.1007/s12613-022-2564-7

Shi-yuan Liu, Yu-lan Zhen, Xiao-bo He, Li-jun Wang, and Kuo-chih Chou, Recovery and separation of Fe and Mn from simulated chlorinated vanadium slag by molten salt electrolysis, *Int. J. Miner. Metall. Mater.*, 27(2020), No. 12, pp. 1678-1686. https://doi.org/10.1007/s12613-020-2140-y

IJMMM WeChat

QQ author group

INTERNATIONAL JOURNAL OF
Minerals, Metallurgy and Materials

Volume 33, Number 2, February 2026
Page 531

Research Article https://doi.org/10.1007/s12613-025-3192-9

Influence of manganese on vanadium precipitation and V_2O_5 purity based on different roasting methods of vanadium slag

Lan Zhang[1)], *Tao Jiang*[1,2,3),✉], *Jing Wen*[1)], *Tangxia Yu*[1)], *Changqing Li*[1)], *and Xinyu An*[1)]

1) School of Metallurgy, Northeastern University, Shenyang 110819, China
2) Laboratory for Ecological Metallurgy of Multimetallic Mineral (Ministry of Education), Northeastern University, Shenyang 110819, China
3) Liaoning Key Laboratory for Metallurgical Sensor and Technology, Shenyang 110819, China
(Received: 15 February 2025; revised: 30 April 2025; accepted: 15 May 2025)

Abstract: Manganese is a major impurity in acidic vanadium-bearing leaching solutions, but its effects on vanadium precipitation via hydrolysis and acidic ammonium salts remain unclear. In this study, vanadium-bearing leachates with varying manganese concentrations (VL-*c*Mn) were prepared through calcium, a calcium–manganese composite, and manganese-based roasting of vanadium slag (VS) to investigate the influence of manganese on vanadium precipitation behavior during hydrolysis precipitation (HP) and ammonium salt precipitation (AP), as well as the microscopic characteristics and purity of the resulting V_2O_5 products. The results showed that increasing the pH mitigated the negative effects of Mn on the V precipitation rate during HP. However, as the manganese concentration increased from 5.69 to 15.38 g/L, the V precipitation rate gradually declined at higher temperatures and longer reaction times. The precipitates exhibited increased microstructural density, which might had contributed to the formation of Mn-bearing phases. Additionally, the average grain size of V_2O_5 was reduced and the particles were increasingly agglomerated, leading to a 2.55% decrease in product purity. For AP, as manganese concentration increased, raising the pH counteracted the negative impact of Mn on the V precipitation rate and reduced the required amount of ammonium sulfate. Moreover, Mn was unevenly adsorbed on the surface of the precipitates. Although V_2O_5 grains gradually shrank and became denser, there was no significant effect on the final product purity, which remained above 99.3%. In conclusion, roasting with added manganese salts influenced the hydrolysis of vanadium but had no significant effect on acidic ammonium salt precipitation.

Keywords: vanadium slag; manganese concentration; hydrolysis precipitation; acidic ammonium salt precipitation; vanadium precipitation rate; vanadium pentoxide purity

1. Introduction

Vanadium is often referred to as the "vitamin of modern industry" owing to its distinctive and significant physical and chemical properties, which make it vital for applications in the steel, aerospace, and battery industries [1–4]. The primary vanadium product, vanadium pentoxide (V_2O_5), is widely used as a raw material for producing energy storage materials, alloys, and photosensitive compounds [5–10]. Approximately 88% of the global annual vanadium production originates from vanadium titanomagnetite (VTM) [11]. In China, the prevailing method for vanadium extraction from VTM is indirect [12], where vanadium is enriched in vanadium slag (VS) through blast furnace ironmaking–vanadium converter oxidation. Consequently, the extraction of vanadium from VS has consistently been the focus of research in the field of vanadium production.

As roasting is the most cost-effective pretreatment method, oxidation roasting is usually performed before the leaching of VS [13]. The purpose of roasting is to decompose and oxidize vanadium–iron spinel in VS at high temperatures and finally convert V^{3+} into pentavalent vanadate [14]. A number of roasting methods have been developed to aid the leaching of VS. Calcium salt brings significant advantages compared with conventional sodium vanadium extraction, for example, lower additives and wastewater treatment costs and easier tailing recovery [15–16]. In addition, acid-soluble manganese vanadate has been identified in the calcified roasting of VS. Inspired by this, our research group and other researchers have proposed and reported new technologies for manganese and calcium–manganese composite roasting [17–22], in which manganese vanadate is generated as the target product and the acidic leaching solution contains a large amount of Mn^{2+}. The introduction of manganese salt not only enabled effective vanadium extraction but also recovered most of the additives. Therefore, clean and efficient pretreatment with calcium and manganese is more suitable for the resource utilization of VS.

Precipitation is indispensable for obtaining vanadium-containing products from acid leaching solutions. The earli-

✉ Corresponding author: Tao Jiang E-mail: jiangt@smm.neu.edu.cn

est application of hydrolysis precipitation (HP) in industrial production was the addition of inorganic acid to adjust the pH, and the vanadium-containing liquid was gradually hydrolyzed to produce hydrated vanadium pentoxide with increasing acidity. HP is simple and inexpensive but suffers from lower product purity [23]. As a result, an acidic precipitation process using ammonium salt as precipitant was proposed, after which the V_2O_5 purity obtained by calcining the precipitated ammonium polyvanadate is as high as 99%, but the ammonia–nitrogen wastewater is difficult to be treated [24–25]. Owing to the advantages of both methods, many scholars have adopted them for preparing V_2O_5 products.

According to previous studies, the V precipitation efficiency and purity of the V_2O_5 product are closely related to the types and concentrations of impurities in the vanadium-containing solutions. Zhang *et al.* [26] directly precipitated calcified leachate via hydrolysis and detected an Mn-containing phase in the hydrolysate. Zhang *et al.* [27] investigated ammonium salt precipitation (AP) of calcified leachate and found that the purity of V_2O_5 product was 98.7% and manganese content was 0.88wt% at manganese concentration of 10 g/L. Wen *et al.* [18] proposed an AP method using Mn leachate and identified Mn as the main impurity in the V_2O_5 product. Based on existing research, Mn is the primary impurity in acidic vanadium-containing leachates derived from the roasting of calcium and manganese salts, which significantly improves the possibility of Mn entering the precipitation products. However, most studies have focused on optimizing HP and AP processes for acidic vanadium-containing leachates. The effects of Mn on the precipitation efficiency of V and the competitive relationship between Mn and V, which react with H^+ and ammonium salts, have not been systematically studied. In addition, the effect of the manganese content on the quality of vanadium products remains insufficiently reported.

Therefore, we employed three roasting mechanisms for VS by adding varying amounts of calcium and manganese carbonates to prepare vanadium-containing liquids with three distinct manganese concentrations. First, the effect of Mn concentration on the V precipitation rate of HP and AP was explored, followed by the characterization of vanadium precipitates before and after calcination, revealing the action mechanism of Mn^{2+} in the precipitates, as well as the effect of Mn concentration on the purity and micromorphology of the V_2O_5 products.

2. Experimental

2.1. Materials

In this study, vanadium slag was sourced from Xichang, Sichuan, China. The chemical composition and main phases are detailed in Table 1 and Fig. 1. The vanadium content in the VS was 14.81wt%, calculated as V_2O_3, and the manganese content was 8.75wt%, calculated as MnO. As shown in Fig. 1, vanadium in VS exists in the spinel phase $(Mn,Fe)(V,Cr)_2O_4$, whereas most of the manganese and iron were present in the spinel as isomorphic substitutions. After roasting, vanadium and manganese in the spinel phase were decomposed into vanadium and manganese oxides, which were further combined to form acid-soluble manganese vanadate.

Analytical-grade reagents $CaCO_3$ and $MnCO_3$ were used as additives to transform stable vanadium spinel into acid-soluble calcium vanadate and manganese vanadate. Other chemical reagents used in the entire process, such as H_2SO_4 and $(NH_4)_2SO_4$ were of analytical grade.

2.2. Method

2.2.1. Preparation of vanadium-containing leachates with different manganese contents

For the calcified and manganised VS processes, the concentration of Mn^{2+} in the vanadium-bearing leaching solution increased with the amount of manganese salt added during the roasting process. Therefore, to prepare vanadium-containing leachates with three manganese contents, we selected the molar ratios of calcium and manganese salt during the actual roasting process of VS [20,28] with $n(CaCO_3)/n(V_2O_3)/n(MnCO_3)$ ratios of 1:1:0 and 0:1:2. Here, n denoted the molar amount of substance (unit: mol). Then, considering the gradient of Mn^{2+} content in the three leachates, combined with the calcium–manganese composite process [18], $n(CaCO_3)/n(V_2O_3)/n(MnCO_3)$ of 0.5:1:1.4 was selected as the roasting additive dosage in the calcium–manganese composite process. The experimental design is summarized in Table 2.

Before roasting, dried VS, $CaCO_3$, and $MnCO_3$ were thoroughly mixed. During roasting, the mixed materials were placed into the muffle furnace at room temperature and heated to 850°C at a rate of 10°C/min. After holding for 120 min, the roasted materials were cooled naturally and ground into powder.

The above roasted samples were leached at 60°C for 60 min with the ratio of liquid volume to solid mass (L/S; mL/g) of 10. Meanwhile, 10vol% H_2SO_4 was continuously

Table 1. Chemical composition of VS wt%

Fe_2O_3	V_2O_3	MnO	CaO	TiO_2	Cr_2O_3	SiO_2	Total
43.12	14.81	8.75	2.47	11.44	2.19	14.30	97.08

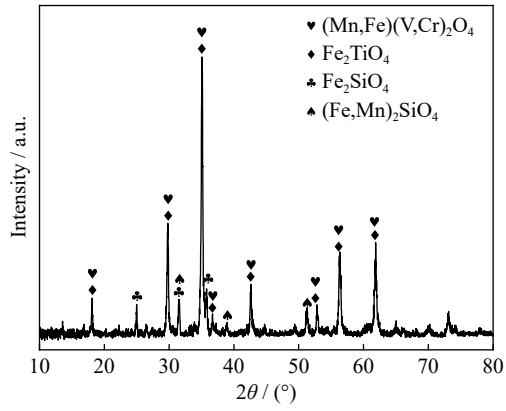

Fig. 1. XRD patterns of VS.

Table 2. Experimental design of different roasting systems

Roasting systems	$n(CaCO_3)$/ $n(V_2O_3)$/$n(MnCO_3)$	Roasting temperature / °C	Roasting time / min	Heating rate / (°C·min^{-1})
Calcification	1:1:0			
Calcium–manganese composite	0.5:1:1.4	850	120	10
Manganese	0:1:2			

added to the leaching system to maintain the pH at 2.5. After leaching, three vanadium-containing leachates were obtained via filtration and separation.

2.2.2. Vanadium precipitation

To examine the effects of manganese on vanadium precipitation characteristics, leaching solutions with different manganese concentrations were used for hydrolysis and acidic ammonium salt precipitation. The sedimentation tests were performed in a thermostatic water bath. For each experiment, 40 mL of leachate was placed in a three-necked flask and stirred.

(1) Hydrolysis.

For hydrolysis precipitation, 20vol% H_2SO_4 was added to adjust the pH to a value between 1.2 and 2.4. The solution was then maintained at this pH for 10–100 min at a temperature of 60–98°C.

(2) Acidic ammonium salt precipitation.

For acidic ammonium salt precipitation, additional $(NH_4)_2SO_4$ was added in a three-necked flask to achieve a mass ratio coefficient K of 0.8–2.2 according to Eq. (1). The coefficient K represents the ratio of ammonium sulfate mass ($m_{(NH_4)_2SO_4}$) to the mass of vanadium in the leachate. Subsequently, 20vol% H_2SO_4 was added to adjust the pH to be between 1.2 and 3.0. The mixture was maintained at this pH for 10–100 min at 80–98°C. Following precipitation, the solid precipitate and wastewater were separated and collected via filtration. The parameters used in these experiments are listed in Table 3. The vanadium precipitation rate (P) was calculated using Eq. (2):

$$K = m_{(NH_4)_2SO_4}/m_{VL} \quad (1)$$

$$P = (1 - m_{VW}/m_{VL}) \times 100\% \quad (2)$$

where m_{VW} and m_{VL} are the masses of vanadium in the wastewater and the vanadium-containing leachate, respectively.

2.2.3. V_2O_5 preparation

The vanadium precipitate was dried in a baking oven at 110°C for 24 h, ground, and calcined at 550°C for 120 min in a muffle furnace to obtain the final V_2O_5 product.

2.2.4. Characterization

The vanadium contents in the leachate and wastewater were determined by the ferrous ammonium sulfate titration method. The concentrations of calcium, manganese, and other ions in the leachate and V_2O_5 products, as well as the chemical composition of VS, were analyzed using inductively coupled plasma atomic emission spectroscopy (ICP-OES, Agilent 5110). X-ray diffraction (XRD, Rigaku Ultima IV) was used to determine the phase composition of solid samples over a 2θ range of 10°–80°. Scanning electron microscopy (SEM, Ultra Plus, Zeiss, Germany) along with energy-dispersive spectroscopy (EDS) was used to observe the microstructure and elemental distribution of the V precipitates and V_2O_5 products.

3. Results and discussion

3.1. Vanadium-containing leachates prepared by different roasting systems

3.1.1. Phase and microscopic analysis of three roasted clinkers

The XRD patterns of the clinkers obtained from different roasting systems were shown in Fig. 2(a). The main phases observed in the roasted products included $(Fe_{0.6}Cr_{0.4})_2O_3$, Fe_2O_3, SiO_2, and Fe_2TiO_5. In addition, vanadate phases such as $Ca_2V_2O_7$ and $Mn_2V_2O_7$ were detected. In the calcified roasting system, the diffraction peaks of $Ca_2V_2O_7$ and $Mn_2V_2O_7$ were present, indicating that manganese in the VS participated in the transformation of vanadium. In the calcium–manganese composite roasting system, the $Mn_2V_2O_7$ diffraction peak was enhanced because of the increase in amount of manganese in VS with the introduction of manganese salt, resulting in manganese competing with calcium for vanadium. However, since the ability of calcium to bind to vanadium is greater than that of manganese, $FeMnO_3$ is formed from the remaining manganese and iron. Roasting at the theoretical molar ratio of $Mn_2V_2O_7$ also resulted in the detection of the $FeMnO_3$ phase in addition to $Mn_2V_2O_7$, further confirming that the manganese in VS participated in the reaction, with an excess of manganese relative to vanadium resulting in a manganese surplus. The production of $Mn_2V_2O_7$ increased with the Mn salt concentration. Fig. 2(b)–(d) illustrates the SEM images and elemental distribution of the roasted VS, where the roasted samples exhibited agglomerated strip and block structures. According to the element distribution map, the distribution areas of Ca and V in calcified roasting were consistent, coexisting with some Mn elements. For calcium–manganese composite roasting, there was an en-

Table 3. Experimental parameters of different precipitation processes

Precipitation process	pH	Temperature / °C	Time / min	K
Hydrolysis	1.2; 1.5; 1.8; 2; 2.2; 2.4	60; 70; 80; 90; 95; 98	10; 20; 40; 60; 100	—
Acidic ammonium salt	1.2; 1.8; 2.2; 2.4; 2.6; 2.8; 3	80; 90; 95; 98	10; 20; 40; 60; 100	0.8; 1; 1.2; 1.5; 1.8; 2.2

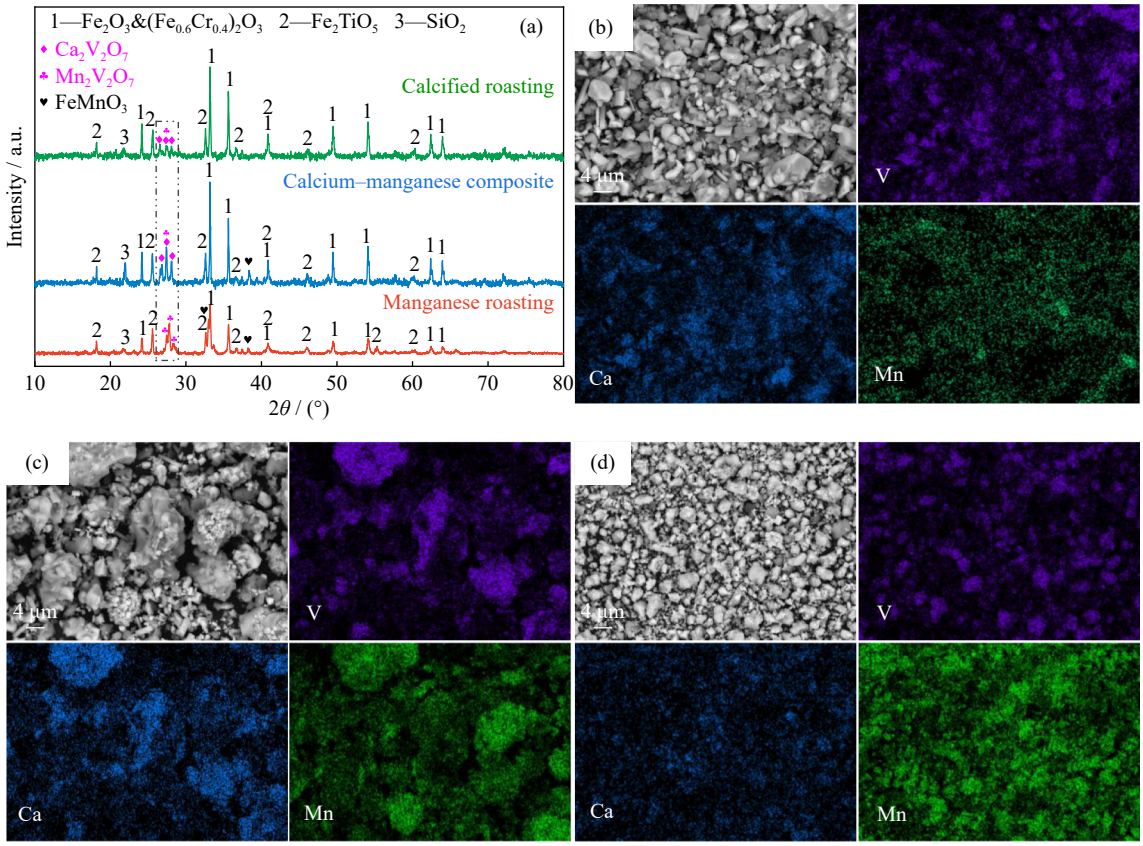

Fig. 2. Characterization of the roasted VS: (a) XRD; (b–d) SEM microstructure and elemental distribution of the clinkers obtained from (b) calcified roasting, (c) calcium–manganese composite roasting, and (d) manganese roasting.

hancement in the areas where V and Mn coexisted. For Mn roasting, the areas corresponding to V and Mn almost overlapped. These results agree with those observed in XRD.

3.1.2. Chemical composition analysis of the three leachates

Sulfuric acid leaching of the three roasted clinkers yielded vanadium-bearing solutions with vanadium concentrations of approximately 15 g/L. The main ion concentrations in the leachates were summarized in Table 4. As shown in Table 4, the Mn^{2+} concentration was 5.69 g/L in the calcified leachate, originating from the dissolution of $Mn_2V_2O_7$ during acid leaching. In the calcium–manganese composite and manganese leachates, the Mn^{2+} concentrations increased to 9.01 and 15.38 g/L, respectively, because of the higher initial manganese salt content, which promoted the formation of more $Mn_2V_2O_7$ during roasting. Most of the Ca^{2+} ions combined with SO_4^{2-} to form $CaSO_4$ during leaching, resulting in relatively lower Ca^{2+} concentrations in the solution. Meanwhile, elements such as Si, Cr, Fe, and Ti primarily remained in the slag phase and their concentrations in the leachates were negligible.

In addition, with the exception of Mn^{2+}, the concentrations of the main ions in the three leachates were similar. Therefore, the change among the precipitate phases, micromorphology, etc. in this experiment could be considered as the influence of a single variable of Mn concentration. For facilitated description, the vanadium-containing leachate obtained after leaching in different roasting systems was expressed as VL-*c*Mn (*c* = 5.69–15.38 g/L).

3.2. Effect of Mn on HP of vanadium

3.2.1. V precipitation rate

Fig. 3 showed the variation of V precipitation rate in VL-*c*Mn with different vanadium precipitation conditions. As shown in Fig. 3(a), under the same manganese concentration, V precipitation rate exhibited a trend of first increase and then decrease as pH value increased from 1.2 to 2.4. When the pH of precipitation was fixed, on increasing the manganese concentration (c_{Mn}) from 5.69 to 15.38 g/L, the trend of change in the precipitation rate of V was not completely consistent. When pH was 1.2, V precipitation rates were less than 84%, which was attributed to re-dissolution of hydrolyzed precipitates at the low pH value [29]. When the pH was increased from 1.2 to 2.0, increasing the manganese concentration led to a reduction in the precipitation rate of V; the

Table 4. Concentrations of main components in leaching liquid (g·L^{-1})

Systems	V	Mn	Ca	Si	Cr	Fe	Ti
Calcification	15.06	5.69	0.78	0.102	2.0×10^{-4}	1.5×10^{-3}	5.0×10^{-4}
Calcium–manganese composite	15.04	9.01	0.77	0.093	3.7×10^{-4}	1.5×10^{-2}	4.5×10^{-4}
Manganese	15.08	15.38	0.76	0.137	4.6×10^{-3}	1.8×10^{-2}	1.0×10^{-2}

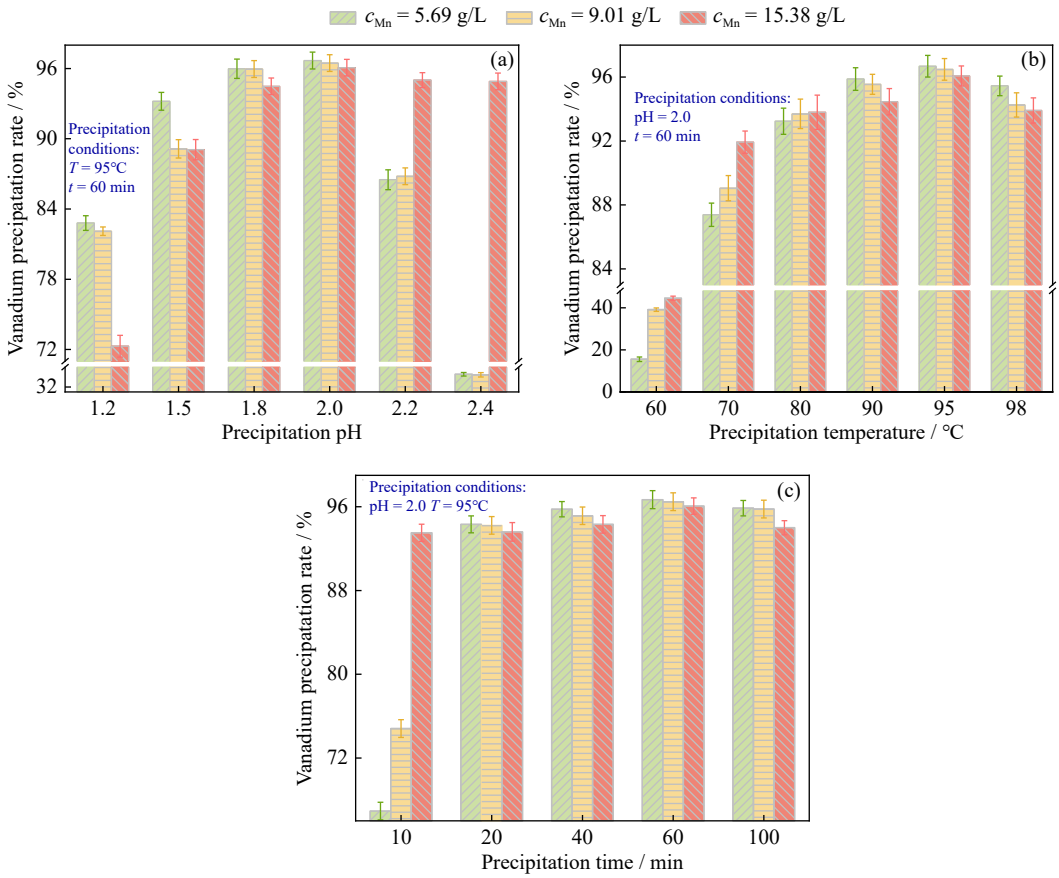

Fig. 3. Vanadium precipitation rates from VL-*c*Mn under varying conditions: (a) effect of precipitation pH; (b) effect of precipitation temperature; (c) effect of precipitation time.

higher the pH, the less was the decrease in precipitation rate of V. When pH was 2.0, V precipitation rate reached the highest value of 96.68%, 96.47%, and 96.07% respectively with the gradual increase of Mn concentration. The results showed that the increase of manganese concentration in leaching solution had an adverse effect on HP, but raising pH value could weaken the negative effect of manganese on V precipitation rate.

It was worth noting that V precipitation rate in leaching solution with Mn concentration less than 10 g/L decreased rapidly to less than 38% when pH continued to increase to 2.4; however, when manganese concentration exceeded 15 g/L, V precipitation rate only decreased slightly and remained above 94.5%. This might be due to the decrease of H^+ in leachate with increasing pH value, where, at the same time, the vanadium-bearing solution with higher manganese content could provide sufficient Mn^{2+} to replace H^+ and combine with vanadate ions, thereby maintaining a relatively high V precipitation rate.

As shown in Fig. 3(b), the precipitation efficiency of V rose sharply on increasing the temperature from 60 to 70°C, reaching 94% at 90°C. With further increase in temperature, the precipitation efficiency of V increased slightly, reaching the maximum at 95°C, and then decreased slightly at 98°C, indicating that an appropriate increase in temperature was conducive to vanadium settlement in HP.

When the temperature was fixed to below 90°C, as the manganese concentration increased, there was an enhancement in the precipitation rate of V to a certain extent. However, the precipitation rate was lower than 94%, which was because of the fact that Mn^{2+} could replace H^+ to participate in HP when a suitable precipitation temperature of filter cake was not reached [30–31], hence the higher the manganese concentration, the greater was the V precipitation rate. However, when the temperature was fixed at 90–98°C, the precipitation rate of V decreased gradually with increasing manganese concentration, indicating that the thermodynamic condition of vanadate ion reacting with H^+ was excellent when temperature exceeded 90°C [30]. At this time, excessive Mn^{2+} in the leachate interfered with HP.

In Fig. 3(c), for a reaction time of 20 min, the precipitation rate of V reached 93%. With increasing reaction time, the increase in the precipitation rate of V was relatively slow, indicating that the reaction rate decreased during the later stages of hydrolysis. The V precipitation efficiency reached its maximum at 60 min, but decreased when extended to 100 min, which was attributed to the re-dissolution of precipitates, resulting in a diminishing vanadium yield.

When the precipitation time was kept constant, an extension of the reaction time from 10 to 20 min leaded to respective increases of 27.39%, 19.40%, and 0.09% in vanadium precipitation efficiency as manganese concentration rose. The Mn concentration had a significant effect on the nucleation rate of the hydrolysates. With increasing Mn^{2+} concen-

tration, the number of crystallization centers increased, accelerating the consumption of vanadate ions and promoting the crystallization of hydrolysates [32]. Furthermore, it elucidated the reason for the good V-precipitation efficiency of VL-15.38Mn at a pH of 2.4, which was attributed to the higher number of crystallization centers in the manganese leachate, promoting the conversion of vanadate ions. In addition, when the reaction time was more than 20 min, the V precipitation rate decreased with an increase in the Mn concentration, indicating that excessive Mn reduced the V precipitation efficiency during the crystal growth of hydrolysates.

In summary, the optimum conditions for HP in VL-*c*Mn were pH = 2.0, temperature (T) = 95°C, and time (t) = 60 min. Under this parameter, the subsequent hydrolysates were characterized to ensure that the Mn concentration was a single variable.

3.2.2. Phase composition and microstructure of precipitates by HP

XRD patterns of hydrolysates of VL-*c*Mn were shown in Fig. 4. As seen in the figure, as manganese concentration increased from 5.69 to 15.38 g/L, the phases of precipitates were essentially the same, composed of amorphous phases and crystalline phases of $MnV_{12}O_{31}\cdot 10H_2O$ and V_2O_5, which proved that the amount of manganese had no effect on the phase composition of hydrolysate. Importantly, the diffraction peaks of $MnV_{12}O_{31}\cdot 10H_2O$ appeared, indicating that some Mn^{2+} in leaching solution would inevitably participate in reaction of HP and replace protons in polymer $H_2V_{12}O_{31}$, as shown in Eqs. (3) and (4) [33–34].

$$6H_2V_{10}O_{28}^{4-} + 24H^+ = 5H_2V_{12}O_{31}(s) + 13H_2O \quad (3)$$

$$H_2V_{12}O_{31} + Mn^{2+} = MnV_{12}O_{31} + 2H^+ \quad (4)$$

The microstructures and elemental distributions of the hydrolysates were shown in Fig. 5. In Fig. 5(a1)–(c1) and (a2)–(c2), the SEM images at different magnifications show that the hydrolysates had irregular block structures. As the Mn concentration increased, there was an increase in the size difference of the grain distributed per unit area and the number of minor fragmented structures, demonstrating that the increase in Mn concentration had a negative impact on the normal growth process of the crystal, but it further verified that it would accelerate nucleation. Meanwhile, the loose

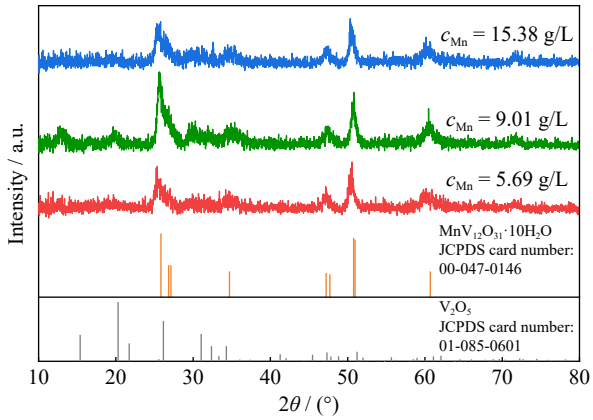

Fig. 4. XRD patterns of hydrolysates obtained from VL-*c*Mn.

porous structure on the surface of the grain gradually decreased, and the density increased successively as the Mn concentration increased, which might have contributed to the formation of Mn-bearing phases. In addition, the distribution area of manganese overlapped with some vanadium and oxygen in the elemental distribution shown in Fig. 5, proving that the Mn^{2+} in the leachates precipitated and transformed. The enrichment of Mn on the particle surface was more significant when there was an increase in the Mn content. The results of EDS analysis of A, B, and C points in Fig. 5 indicate that V, Mn, and O were the main elements at those points, and the Mn content in hydrolysates was increased from 2.77wt% to 4.65wt%, which further confirmed the increase of Mn in precipitates with the addition of manganese concentration in leachates.

3.2.3. V_2O_5 product

As shown in Fig. 6, the V_2O_5 phase was the main phase in the hydrolysates after calcination. However, a small number of low-intensity diffraction peaks of MnV_2O_6 were also detected, indicating that the Mn-bearing phase in the hydrolysate exhibited the MnV_2O_6 phase after calcination. Meanwhile, the diffraction peak intensity of V_2O_5 faded as the manganese concentration increased, suggesting a declining amount of V_2O_5.

The calcined products were analyzed by SEM–EDS to investigate the influence of the manganese concentration on the microstructure of the V_2O_5 products. In Fig. 7(a1)–(c2), the SEM images at different magnifications show that V_2O_5 existed in a rod-like structure. With increasing Mn content, the average size of the V_2O_5 grains gradually decreased, the grain distribution became denser, and agglomeration became severe. When the Mn concentration exceeded 15 g/L, the crystal defects of V_2O_5 were pronounced, revealing that the interactions between the vanadate ions binding to Mn^{2+} and the reaction of vanadate ions with H^+ were mutually influential, thereby obstructing the normal growth of V_2O_5 crystals. The EDS analysis of points a, b, and c in Fig. 7 displayed that there were tiny amounts of Ca and Mn in the products, except for V and O, and that manganese increased with increasing manganese concentration in the leachates.

Furthermore, to clarify the effect of the concentration of manganese on the quality of the V_2O_5 products, the contents of V, Mn, and Ca in the products were analyzed by ICP. It can be seen from Fig. 8, the product purity of VL-5.69Mn was 95.2%; however, the purity of VL-15.38Mn reduced to 92.65%, in consistency with the XRD results shown in Fig. 6. As the concentration of manganese increased, the change in trend of manganese content was opposite to that of vanadium, enhancing from 2.57wt% to 5.11wt%. It was confirmed that the Mn content in the HP increased as the Mn concentration increased. Moreover, the calcium content in the products decreased, but overall, it remained lower than that of manganese owing to the higher manganese concentration in the leachate compared to calcium. Elevated levels of Mn^{2+} in the leachate weakened the binding of vanadium to calcium during the HP process, while enhancing the reaction

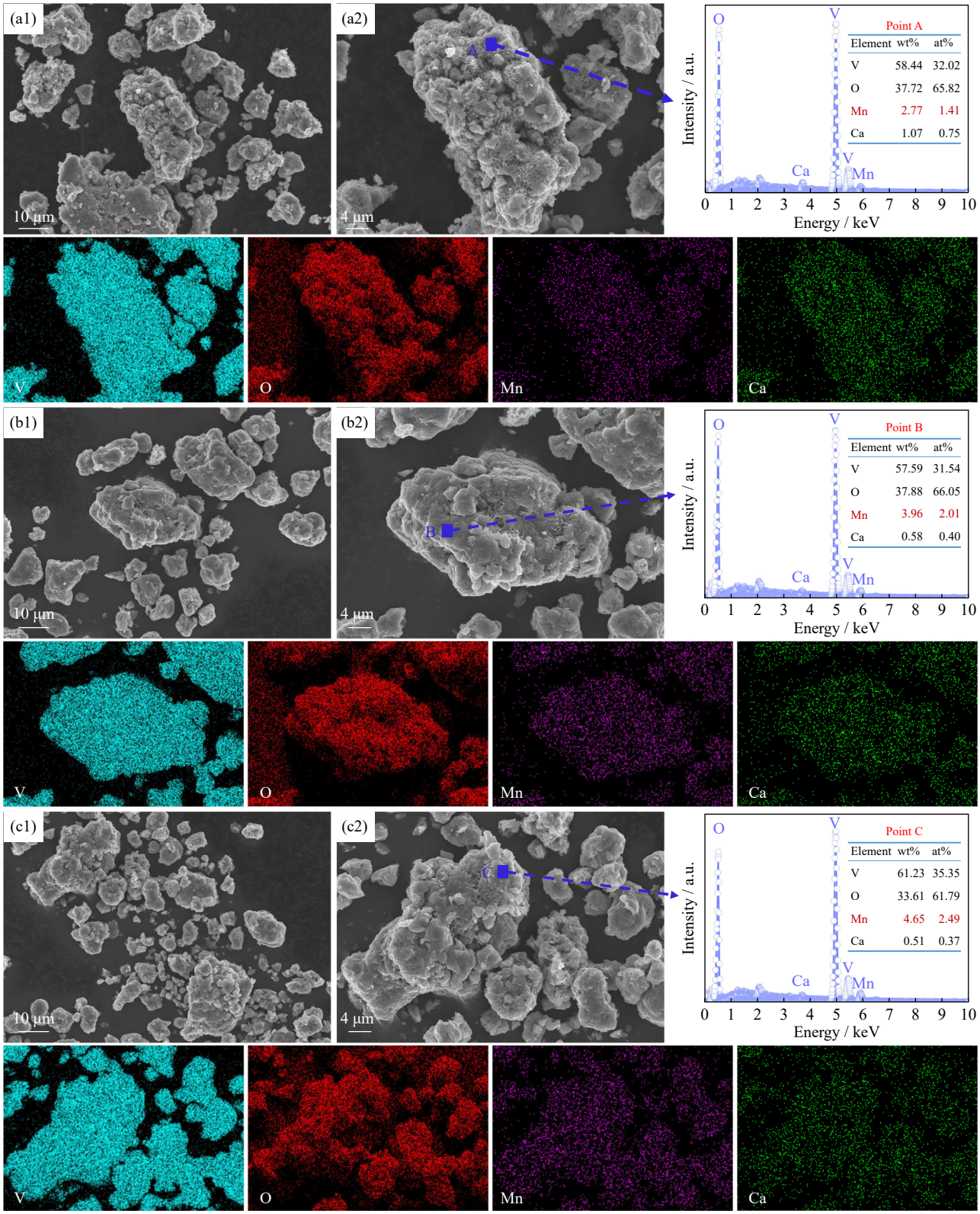

Fig. 5. SEM–EDS analyses of hydrolysates obtained from VL-*c*Mn: (a1, a2) c_{Mn} = 5.69 g/L; (b1, b2) c_{Mn} = 9.01 g/L; (c1, c2) c_{Mn} = 15.38 g/L.

between vanadium and manganese.

3.3. Effect of Mn on AP of vanadium

3.3.1. V precipitation rate

As shown in Fig. 9, when the Mn concentration was fixed, as the pH increased from 1.2 to 3.0, the V precipitation rate exhibited a trend where it first increased and then decreased, reaching a maximum value when the pH value was 2.6 or 2.8. At the same pH, as the Mn concentration increased, the change in the V precipitation rate was inconsistent. When pH was 1.2, the precipitation rate of V was below 72% owing to the fact that higher acidity was unfavorable for reaction of

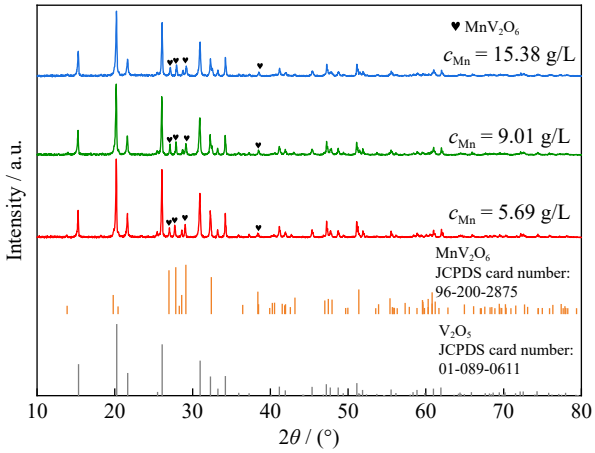

Fig. 6. XRD patterns of calcined hydrolysates obtained from VL-*c*Mn.

vanadate ions with NH_4^+ to produce insoluble vanadium precipitates [27,35].

In the process of increasing the pH value from 1.2 to 2.2, the precipitation rate of V gradually decreased with increasing Mn concentration. However, at pH of 2.4, the V precipitation rates of VL-*c*Mn were essentially the same. As the pH continued to increase, the V precipitation rates of leachates with Mn concentrations lower than 10 g/L and higher than 15 g/L reached their limits at pH 2.6 and 2.8, respectively. Nevertheless, when pH reached 3, V precipitation rate decreased; the higher the manganese concentration, the smaller was reduction in the precipitation rate of V—the V precipitation rate of VL-5.69Mn dropped abruptly from 97% to 40.35%, whereas VL-15.38Mn still reached 98%. Consequently, the disadvantageous effects of Mn could be mitigated by properly increasing the pH value, thereby improving the V precipitation efficiency of the vanadium liquor with a high manganese concentration.

To further explore the influence of the Mn concentration on the most suitable parameters and optimal V precipitation rate for AP, the optimum precipitation temperature, dosage of ammonium sulfate, and time of VL-*c*Mn were investigated at the optimal pH value. The results were presented in Fig. 10(a)–(c).

As shown in Fig. 10(a), the V precipitation rate rose with increasing temperature at the same manganese concentration. Vanadium was hardly precipitated at 80°C. When temperature enhanced to 90°C, with the increase of manganese concentration from 5.69 to 15.38 g/L, V precipitation rate reached 96.44%, 89.36%, and 8.31%, severally. When temperature raised to 98°C, the V precipitation rate reached peak, which were 98.66%, 98.12%, and 99.10% respectively, increasing by 2.22%, 8.76%, and 90.79%. It was shown that the requirements for temperature of AP became more strin-

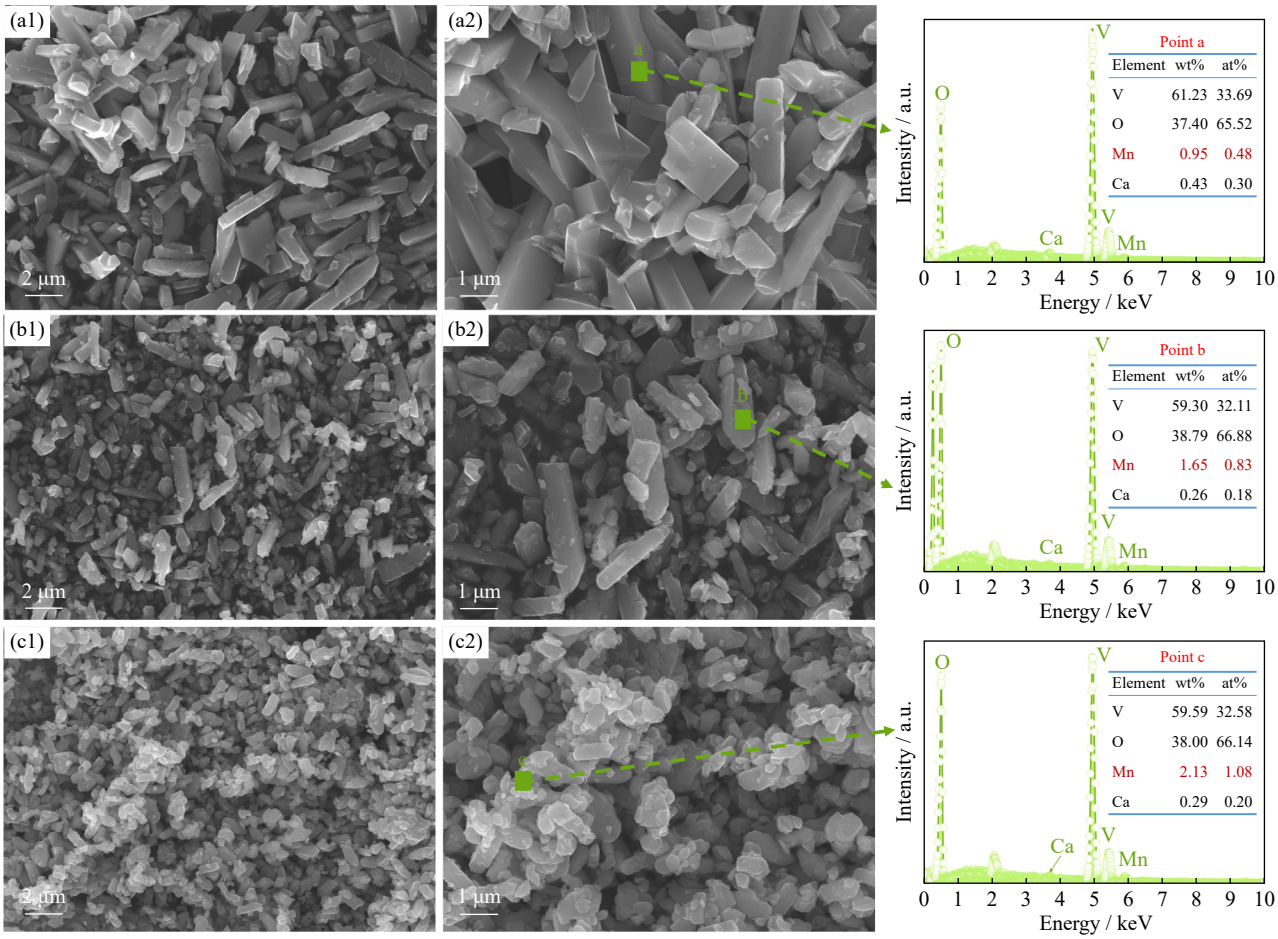

Fig. 7. SEM–EDS analyses of calcined hydrolysates obtained from VL-*c*Mn: (a1, a2) c_{Mn} = 5.69 g/L; (b1, b2) c_{Mn} = 9.01 g/L; (c1, c2) c_{Mn} = 15.38 g/L.

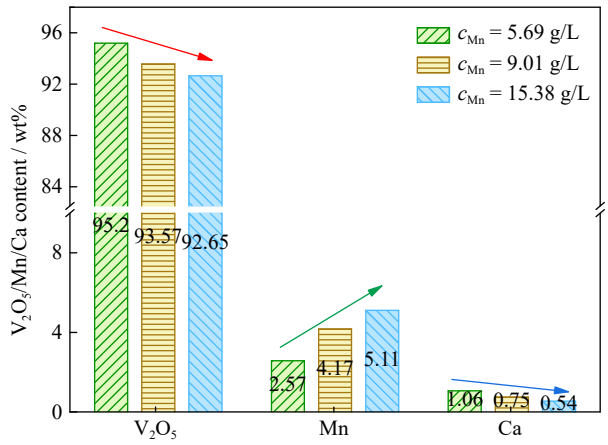

Fig. 8. Contents of V, Mn, and Ca in calcined hydrolysates derived from VL-*c*Mn.

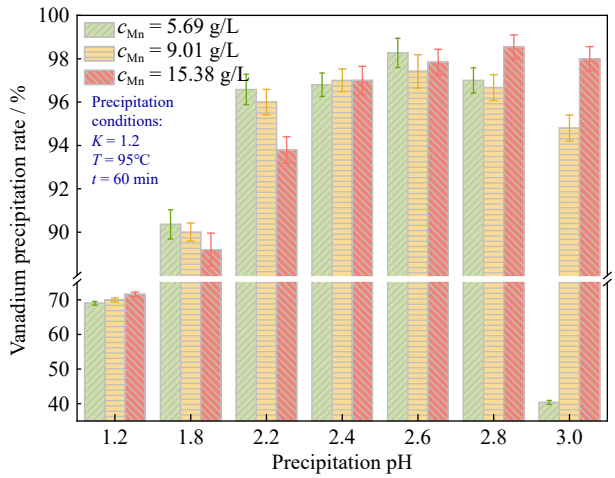

Fig. 9. Vanadium precipitation rate of VL-*c*Mn under different pH values during AP.

gent as manganese concentration increased and pH value rose. Furthermore, on comparing Fig. 10(a) and Fig. 3(b), it was revealed that the hydrolysis reaction approached equilibrium at temperature above 90°C; when temperature was higher than 95°C, the reaction of AP was relatively complete. Thus, higher temperatures should be provided to the AP for favorable reactions.

As shown in Fig. 10(b), at various Mn concentrations, the V-precipitation rate increases with the addition of ammonium sulfate. V precipitation rate of VL-5.69Mn reached 99.08% at K = 1.5, and further addition of ammonium sulfate led to a minor increase in V precipitation rate. V precipitation rate of VL-9.01Mn initially exceeded 99% at K = 1.8,

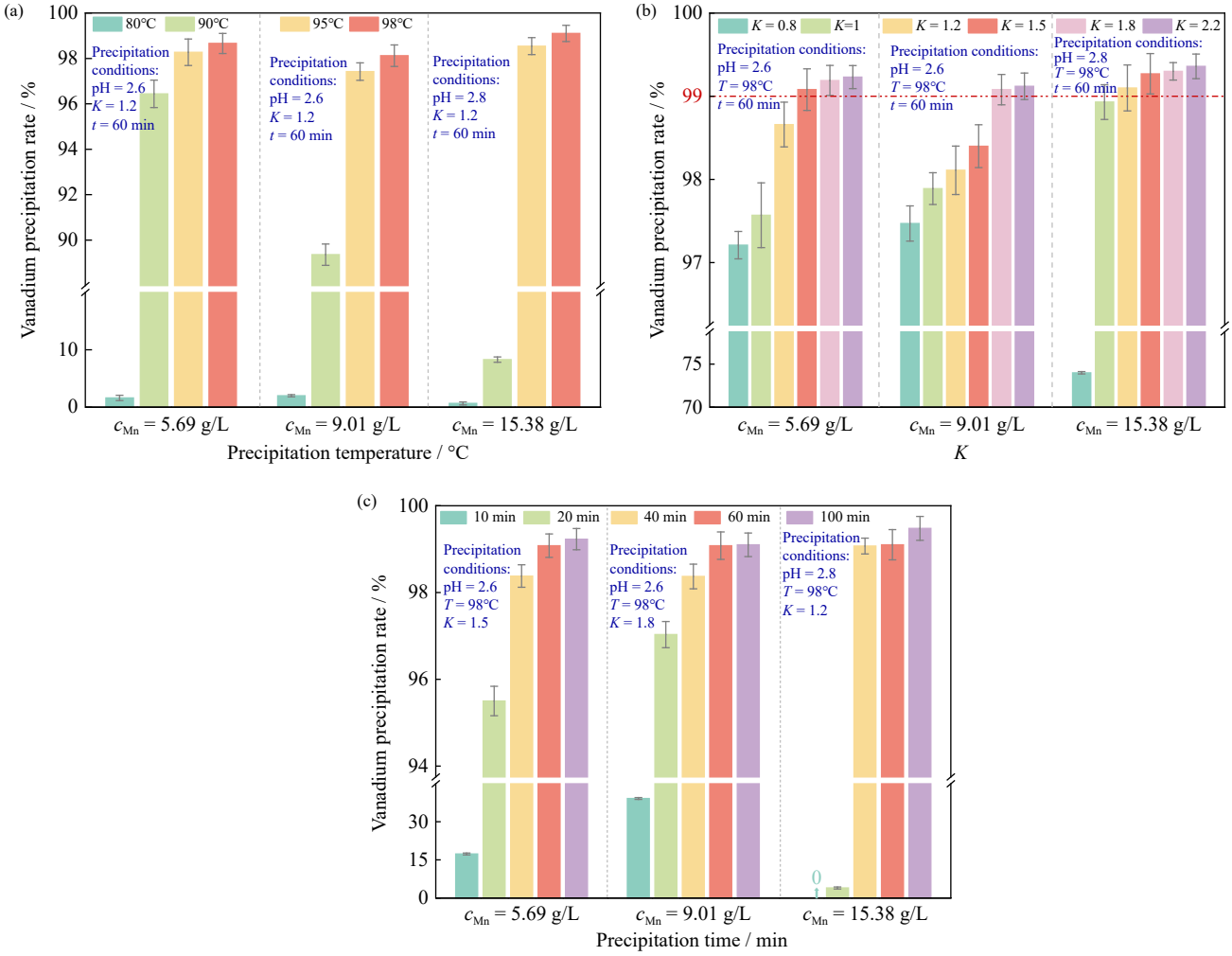

Fig. 10. Vanadium precipitation rate during ammonium salt precipitation of VL-*c*Mn under different conditions: (a) precipitation temperature; (b) *K*; (c) precipitation time.

demonstrating that the addition of ammonium sulfate could improve V precipitation rate, enabling the elimination of the deteriorating effect of Mn concentration on V precipitation rate. Importantly, when pH was 2.8, V precipitation rate of VL-15.38Mn exceeding 99% could be achieved even with *K* of only 1.2, indicating that increasing the pH value of acidic ammonium salt precipitation could increase the vanadium precipitation rate and reduce the dosage of ammonium sulfate for vanadium solutions with high manganese concentrations. At this time, the AP conditions were more moderate, resulting in cost reduction without affecting the V precipitation rate.

As shown in Fig. 10(c), fixing manganese concentrations, V precipitation rate rose with the extension of precipitation time. When the time reached 60 min, V precipitation rate was above 99%. Continuing to prolong reaction time resulted in almost no change; hence, 60 min was selected as the most suitable precipitation time. Under the optimal precipitation parameters of vanadium, V precipitation rate of VL-*c*Mn exceeded 99%.

Comparing Fig. 10(c) and Fig. 3(c), the V precipitation rate of HP was markedly higher than that of AP at a reaction time of 10 min, indicating that the nucleation rate of the ammonium polyvanadate crystals was slower than that of the hydrated V_2O_5. In addition, by prolonging the time of AP, the filter cake did not dissolve back, destroying the precipitation effect, which differed from HP.

3.3.2. Phase composition and microstructure of precipitates by AP

To explore the effect of manganese concentration in leaching solution on the phase composition and microstructure of vanadium-containing precipitates by AP, the precipitates of AP for 60 min at pH of 2.6, temperature of 95°C, and *K* of 1.2 were analyzed by XRD and SEM and the results were shown in Fig. 11 and Fig. 12.

In Fig. 11, when manganese concentration increased from 5.69 to 15.38 g/L, the phase composition and crystallinity of vanadium cake did not change, shown as hexameric ammonium vanadate with high crystallinity, which was consistent with the standard card of $(NH_4)_2V_6O_{16}$ (JCPDS card number: 01-079-2051), revealing that the difference in manganese content would not affect the mutual reaction types of each component in precipitation process.

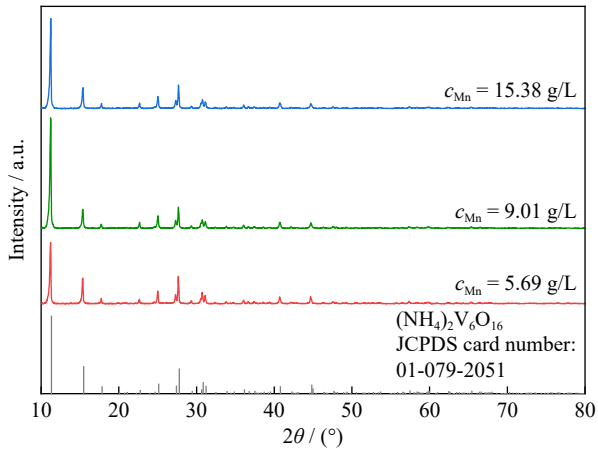

Fig. 11. XRD patterns of ammonium salt precipitates derived from VL-*c*Mn.

The reactions for AP are shown in Eq. (5). NH_4^+ has a strong binding force with vanadate ions; therefore, it replaces H^+ to form an ammonium vanadate precipitate. Meanwhile, according to the order of vanadium affinity for different cations, $K^+ > NH_4^+ > H^+ > Na^+ > Ca^{2+} \approx Mn^{2+}$ [29], it was found that the binding ability of Mn^{2+} for vanadium was much lower than NH_4^+. Hence, it is difficult for Mn^{2+} to form complexes with vanadate ions in the case of abundant NH_4^+. Thus, no diffraction peaks of the other vanadates were detected in the precipitates.

$$0.6H_2V_{10}O_{28}^{4-} + 0.4H^+ + 2NH_4^+ = (NH_4)_2V_6O_{16}(s) + 0.8H_2O \quad (5)$$

Fig. 12 displays the microstructure and elemental distribution of the AP precipitates at different magnifications. As shown in the figure, the particles are composed of flaky crystals of different sizes that are embedded in each other. Moreover, as the Mn concentration increased, the particle roughness and irregularity increased, indicating that the crystal growth process was impeded by increasing Mn concentration.

According to the elemental distributions shown in Fig. 12, the distribution areas of V, N, and O were highly coincident, verifying that vanadium was converted into ammonium polyvanadate and entered the filter cake during the AP process. Mn and Ca were scattered on the surfaces of the particles and were present in extremely small amounts. Combined with EDS analysis results of points D, E, and F shown in Fig. 12, it was found that the total content of Mn and Ca was less than 0.3wt%, except V, N, and O. Besides, with increasing Mn concentration in leaching solution, Mn content on the surface of particles increased slightly from 0.14wt% to 0.26wt%. It is worth noting the lack of correlation between Mn and other elements because no Mn-bearing phase was detected in Fig. 11, implying that Mn was unevenly adsorbed on the surface of the filter cake.

3.3.3. V_2O_5 product

To investigate the effect of Mn concentration on the phase composition of vanadium products formed by AP, the calcined precipitates were analyzed by XRD, as shown in Fig. 13. After calcination, the AP precipitates decomposed and deaminated to obtain V_2O_5, and the position and intensity of the synthesized V_2O_5 peaks were consistent with the standard card of V_2O_5 (JCPDS card number: 01-089-0611). Furthermore, despite the introduction of higher amounts of Mn^{2+} into the leachate, no other diffraction peaks were detected, except for V_2O_5, indicating that the manganese concentration did not affect the phase composition of the precipitates because of the strong selectivity of NH_4^+ for vanadium.

The microstructures of V_2O_5 products were further observed, and the results are shown in Fig. 14. In Fig. 14(a1)–(c2), SEM images at different magnifications show that V_2O_5 existed in rod-like structures. As the Mn concen-

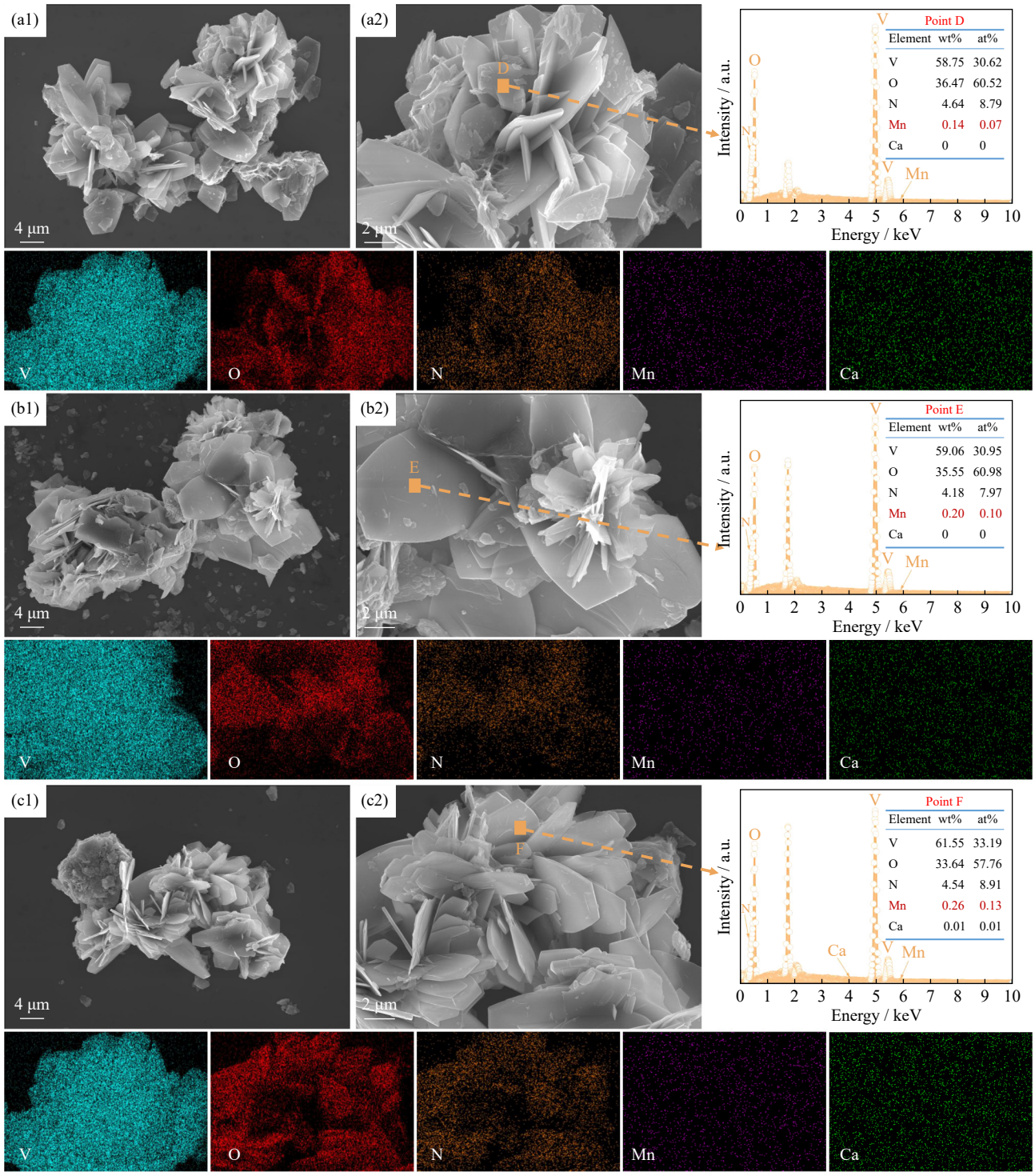

Fig. 12. SEM–EDS analyses of ammonium salt precipitates of VL-*c*Mn: (a1, a2) c_{Mn} = 5.69 g/L; (b1, b2) c_{Mn} = 9.01 g/L; (c1, c2) c_{Mn} = 15.38 g/L.

tration increased, the grain size of V_2O_5 gradually decreased. When the manganese concentration was higher than 9 g/L, the degree of crystal defects increased, and the difference in morphology and size between grains was remarkable. When manganese concentration exceeded 15 g/L, the phenomenon of grain agglomeration was serious, and major grain sharply shrunk to less than 1 μm, which demonstrated that Mn^{2+} in leaching solution would disrupt with the formation and growth process of ammonium polyvanadate (APV) crystals. From the results of the EDS analysis of points d, e, and f in Fig. 14, it can be observed that the peak intensities of manganese and calcium in the energy spectrum were relatively weak, and the mass content was low, proving that the impurities of manganese and calcium in the V_2O_5 products were lower, in consistent with the results of the EDS analyses in Fig. 12.

To further explore the effect of Mn concentration on the quality of the vanadium products produced by AP, the contents of V, Mn, and Ca in the products were analyzed by ICP, and the results are depicted in Fig. 15. It could be seen that

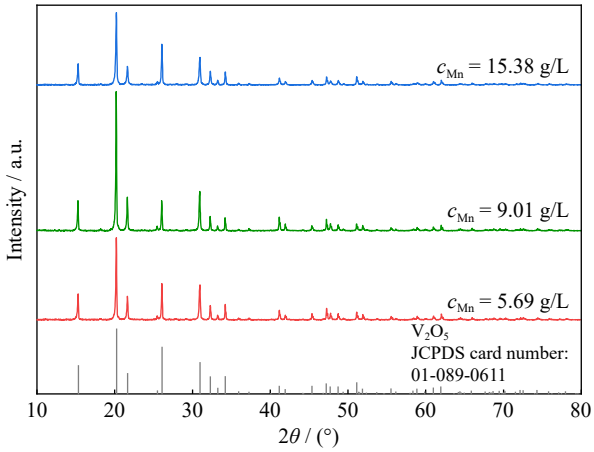

Fig. 13. XRD patterns of calcined ammonium salt precipitates of VL-*c*Mn.

the contents of V_2O_5 prepared by VL-*c*Mn were comparable with all above 99wt%, reaching the standard of Grade 99 V_2O_5 product in YB/T5304-2011. With increasing Mn concentration, the Mn content of V_2O_5 product raised slightly. On the contrary, calcium content decreased slightly, but the total impurity content was less than 0.7wt%, implying that manganese concentration had a relatively small influence on the purity of V_2O_5 product obtained using AP. Moreover, compared with HP, the vanadium products prepared using AP had a higher purity, and the manganese impurity content was much lower. In other words, pretreatment of the calcium–manganese composite and manganese roasting hardly affected the quality of the V products obtained from AP.

3.4. Comparison of action mechanism of manganese in HP and AP processes

The mechanisms of action of Mn in the HP and AP processes are shown in Fig. 16. During the HP process, some Mn competed with H^+ for a spot of vanadium, resulting in Mn participating in precipitation and entering the precipitate. After calcination, manganese existed as manganese vanadate in the V_2O_5 product. In the AP process, the binding ability of NH_4^+ to vanadium was strong; hence, manganese dropped out of the precipitate and was merely adsorbed onto the surface of the precipitant, and trace amounts of manganese were eventually attached to the surface of the calcined product.

4. Conclusions

In this study, three vanadium-containing leachates with varying Mn concentrations were prepared via leaching after three different roasting methods to investigate the influence of Mn content on V precipitation characteristics and product quality. The main conclusions were as follows:

(1) For HP, increasing the pH mitigated the adverse effect of Mn on V precipitation rate. However, at higher precipita-

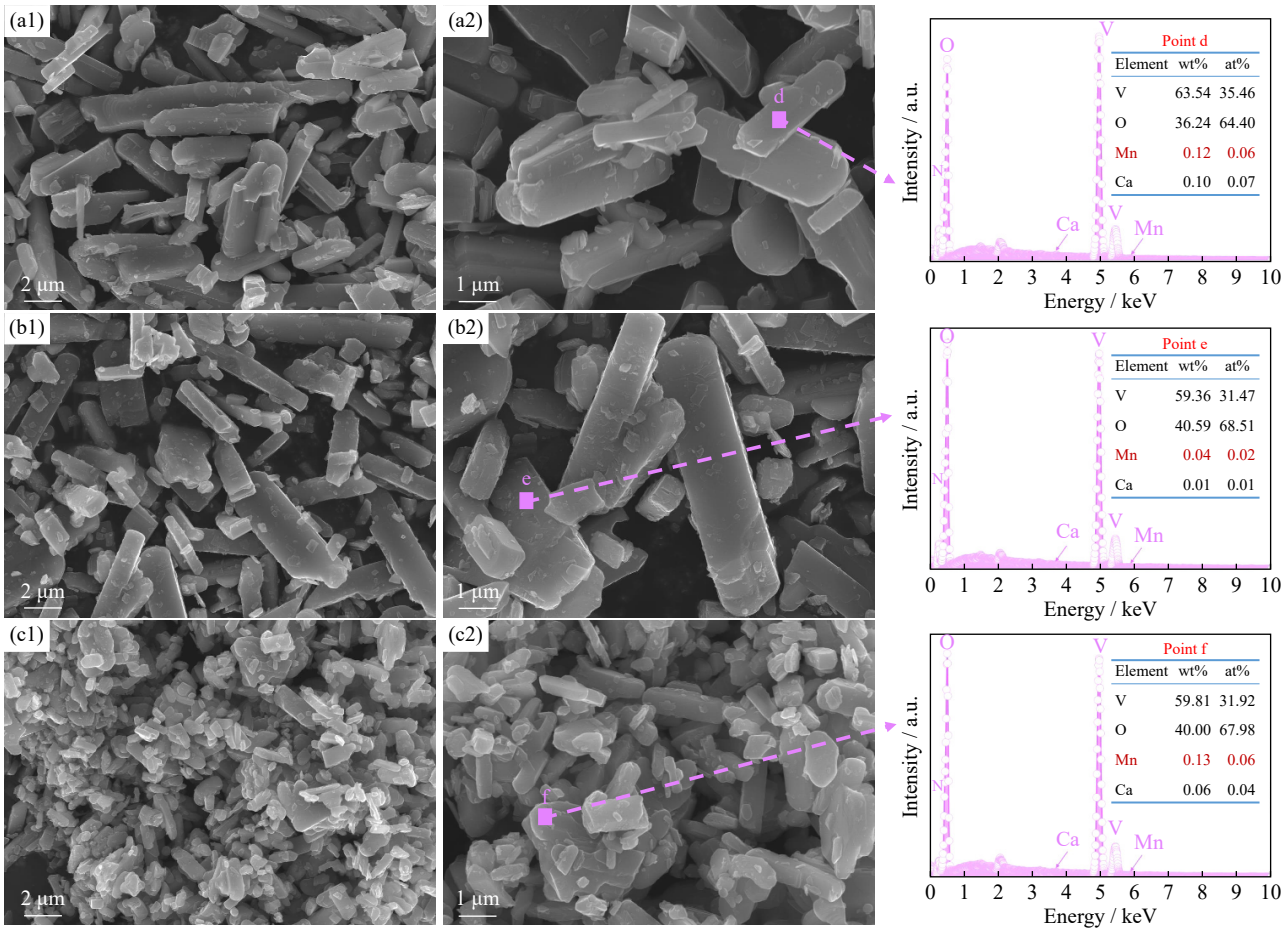

Fig. 14. SEM–EDS analyses of calcined ammonium salt precipitates of VL-*c*Mn: (a1, a2) c_{Mn} = 5.69 g/L; (b1, b2) c_{Mn} = 9.01 g/L; (c1, c2) c_{Mn} = 15.38 g/L.

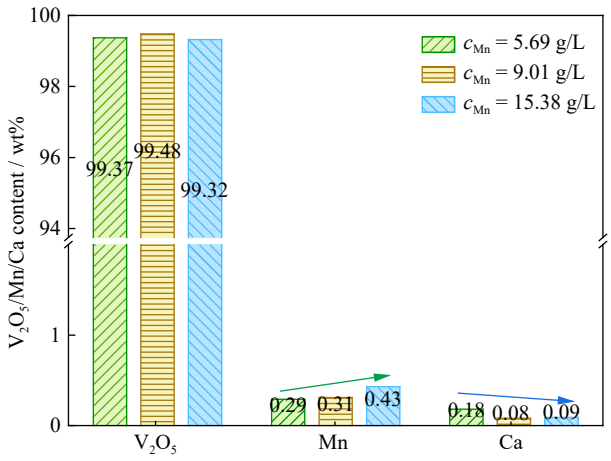

Fig. 15. Contents of V, Mn, and Ca in calcined ammonium salt precipitates of VL-*c*Mn.

tion temperatures and longer reaction times, the V precipitation rate gradually decreased with increasing Mn concentration. For the AP, increasing the pH eliminated the deteriorating effect of Mn on V precipitation and reduced the required amount $(NH_4)_2SO_4$.

(2) The main phases of HP precipitates from VL-*c*Mn remained largely consistent regardless of Mn concentration; however, the higher Mn levels led to denser precipitates, likely because of the formation of Mn-bearing phases. Similarly, the phase composition and crystallinity of AP precipitates remained stable, though Mn was unevenly adsorbed on the grains' particle surfaces, which increased surface roughness and irregularity.

(3) MnV_2O_6 was consistently detected in V_2O_5 products obtained by HP. Increasing Mn concentration resulted in smaller particle sizes, particle agglomeration, and a gradual decline in product purity. In contrast, no Mn-bearing phases were found in V_2O_5 products from AP. The grain size decreased, and particle distribution became denser, but product purity remained high, above 99.3%.

Acknowledgements

This work was financially supported by National Natural Science Foundation of China (Nos. 52204309, 52174277 and 52374300), and Fundamental Funds for the Central Universities (No. N2425026)

Conflict of Interest

The authors declare that they have no known competing financial interests or personal relationships that could have appeared to influence the work reported in this paper.

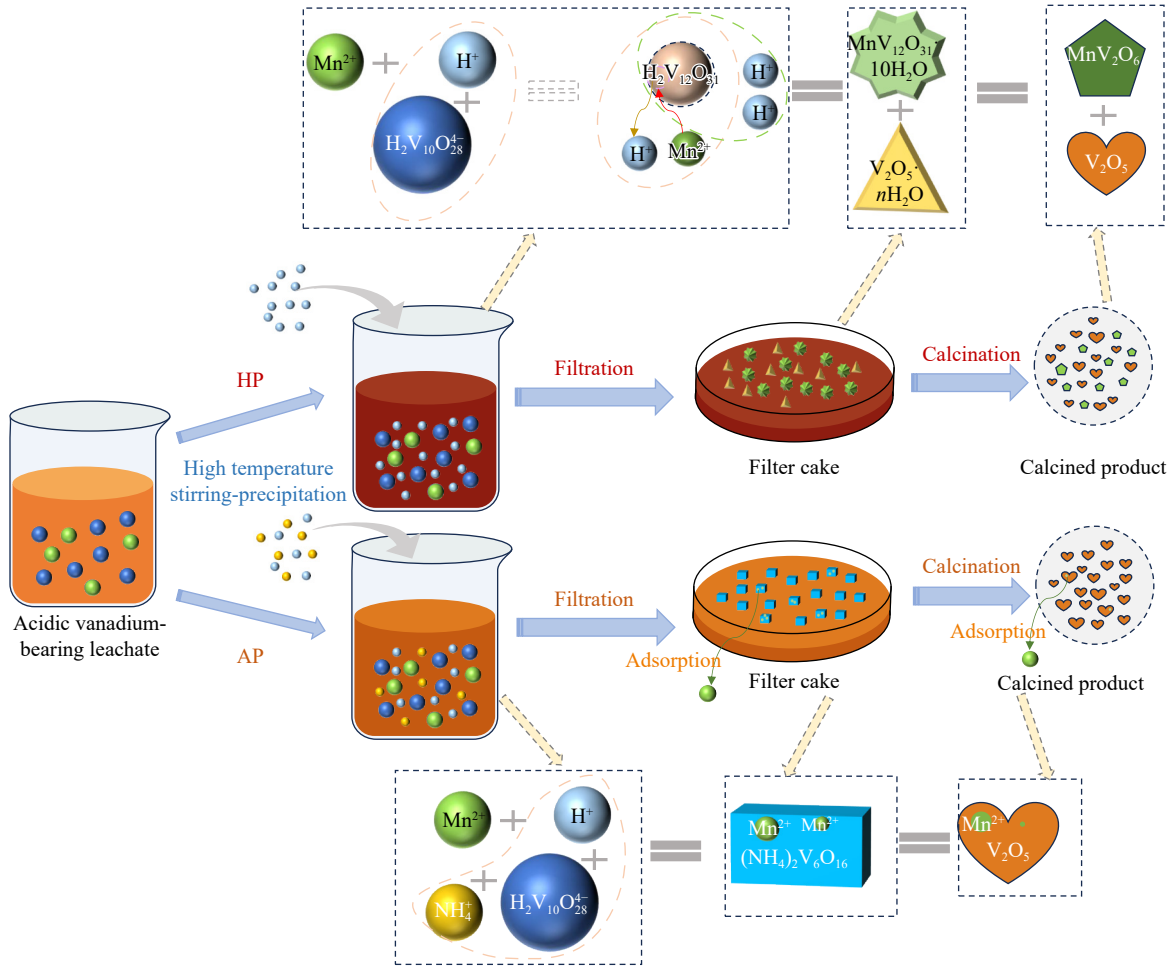

Fig. 16. Schematic illustration of the role and mechanism of Mn in V precipitation during HP and AP processes.

References

[1] S. Kumar, A. Jain, T. Ichikawa, Y. Kojima, and G.K. Dey, Development of vanadium based hydrogen storage material: A review, *Renewable Sustainable Energy Rev.*, 72(2017), p. 791.

[2] X.S. Li, *Mechanism Research on Oxidation Roasting and Leaching Process of High Calcium Low-Grade Vanadium Slag* [Dissertation], Chongqing University, Chongqing, 2011, p. 2.

[3] S.Y. Liu, L.J. Wang, J. Chen, L. Ye, and J.Y. Du, Research progress of vanadium extraction processes from vanadium slag: A review, *Sep. Purif. Technol.*, 342(2024), art. No. 127035.

[4] J.J. Shi, Y.M. Zhai, Y.C. Qiu, *et al*., Phase equilibria relations in the V_2O_5-rich part of the Fe_2O_3–TiO_2–V_2O_5 system at 1200°C related to converter vanadium-bearing slag, *Int. J. Miner. Metall. Mater.*, 31(2024), No. 9, p. 2017.

[5] J.Y. Xiang, X. Lu, L.W. Bai, *et al*., Oxidation behavior of FeV_2O_4 and $FeCr_2O_4$ particles in the air: Nonisothermal kinetic and reaction mechanism, *Int. J. Miner. Metall. Mater.*, 31(2024), No. 8, p. 1839.

[6] G.L. Wang, J.Q. Wang, J.L. Song, *et al*., High-energy-density all-V_2O_5 battery, *Small*, 20(2024), No. 51, art. No. 2407159.

[7] H.C. Prakash, M.S. Kumar, T.W. Lin, and S.K. Batabyal, Photo-assisted capacitive performance of V_2O_5 supercapacitor, *Electrochim. Acta*, 469(2023), art. No. 143229.

[8] Y.Q. Ma, X.W. Wang, S. Stopic, *et al*., Preparation of vanadium oxides from a vanadium (IV) strip liquor extracted from vanadium-bearing shale using an eco-friendly method, *Metals*, 8(2018), No. 12, art. No. 994.

[9] I.E. Kolesnikov, D.V. Mamonova, M.A. Kurochkin, E.Y. Kolesnikov, and E. Lähderanta, Optical thermometry by monitoring dual emissions from YVO_4 and Eu^{3+} in YVO_4:Eu^{3+} nanoparticles, *ACS Appl. Nano Mater.*, 4(2021), No. 2, p. 1959.

[10] N. Jeeva, K. Thirunavukkarasu, and J.R. Xavier, Influence of multifunctional graphene oxide and silanized vanadium nitride in polyurethane coatings for the protection of aluminium alloy in aerospace industries, *Diam. Relat. Mater.*, 142(2024), art. No. 110792.

[11] A. Volkov, U. Kologrieva, A. Kovalev, D. Wainstein, and V. Vakhrushev, Vanadium chemical compounds forms in wastes of vanadium pentoxide production, *Materials*, 13(2020), No. 21, art. No. 4889.

[12] Y.H. Wang, Y.F. Wang, Y.T. Li, *et al*., A review on vanadium extraction techniques from major vanadium-containing resources, *Rare Met.*, 43(2024), No. 9, p. 4115.

[13] J. Wen, T. Jiang, M. Zhou, H.Y. Gao, J.Y. Liu, and X.X. Xue, Roasting and leaching behaviors of vanadium and chromium in calcification roasting–acid leaching of high-chromium vanadium slag, *Int. J. Miner. Metall. Mater.*, 25(2018), No. 5, p. 515.

[14] H. Peng, A literature review on leaching and recovery of vanadium, *J. Environ. Chem. Eng.*, 7(2019), No. 5, art. No. 103313.

[15] J. Wen, T. Jiang, Y.J. Liu, and X.X. Xue, Extraction behavior of vanadium and chromium by calcification roasting–acid leaching from high chromium vanadium slag: Optimization using response surface methodology, *Miner. Process. Extr. Metall. Rev.*, 40(2019), No. 1, p. 56.

[16] J. Wen, T. Jiang, X.L. Zheng, J.P. Wang, J. Cao, and M. Zhou, Efficient separation of chromium and vanadium by calcification roasting–sodium carbonate leaching from high chromium vanadium slag and V_2O_5 preparation, *Sep. Purif. Technol.*, 230(2020), art. No. 115881.

[17] J. Wen, T. Jiang, J.P. Wang, L.G. Lu, and H.Y. Sun, Cleaner extraction of vanadium from vanadium–chromium slag based on MnO_2 roasting and manganese recycle, *J. Cleaner Prod.*, 261(2020), art. No. 121205.

[18] J. Wen, T. Jiang, J.P. Wang, H.Y. Gao, and L.G. Lu, An efficient utilization of high chromium vanadium slag: Extraction of vanadium based on manganese carbonate roasting and detoxification processing of chromium-containing tailings, *J. Hazard. Mater.*, 378(2019), art. No. 120733.

[19] F.F. Li, J. Wen, T. Jiang, C.Q. Li, and H. Xiao, Study on leaching behavior of vanadium in acid leaching process of calcium and manganese vanadate system, *Iron Steel Vanadium Titanium*, 45(2024), No. 3, p. 16.

[20] J. Wen, T. Jiang, T.X. Yu, B.J. Chen, and L. Li, Clean and efficient extraction of vanadium from vanadium slag: Effect of manganese on the phase composition and vanadium extraction process, *J. Cleaner Prod.*, 367(2022), art. No. 133077.

[21] J. Wen, H.Y. Sun, T. Jiang, B.J. Chen, F.F. Li, and M.X. Liu, Comparison of the interface reaction behaviors of CaO–V_2O_5 and MnO_2–V_2O_5 solid-state systems based on the diffusion couple method, *Int. J. Miner. Metall. Mater.*, 30(2023), No. 5, p. 834.

[22] S. Xiao, *Study on the Roasting Behavior of the Converter Vanadium Slag with MnO_2 and the Process of Compound Roasting-Acid Leaching Process* [Dissertation], Chongqing University, Chongqing, 2021, p. 40.

[23] Z.H. Wang, L. Chen, Z.F. Qin, *et al*., Tuning the nucleation rates for high-efficiency hydrolysis of sodium vanadate solution, *Ind. Eng. Chem. Res.*, 62(2023), No. 28, p. 11128.

[24] G.C. Lin, J. Huang, Y.M. Zhang, and P.C. Hu, A sustainable technique to prepare high-purity vanadium pentoxide via purification with low ammonium consumption, *Materials*, 15(2022), No. 5, art. No. 1945.

[25] Q.Q. Zheng, Y.M. Zhang, J. Huang, and S.X. Bao, Study on treatment of high concentration ammonia nitrogen wastewater from vanadium shale extraction by stripping-ion exchange coupling process, *Nonferrous Met. Extr. Metall.*, (2019), No. 6, p. 67.

[26] G.Q. Zhang, R. Tao, Z.F. Qin, and S. Peng, Preparation of high-purity V_2O_5 using an acidic vanadium slag leaching solution from calcification roasting, *Chin. J. Rare Met.*, 45(2021), No. 1, p. 70.

[27] J.H. Zhang, Z.F. Yan, and L. Zhang, Influence factors and kinetics of vanadium precipitation for the vanadium solution from calcified vanadium extraction, *Chin. J. Process. Eng.*, 18(2018), No. 1, p. 111.

[28] T.X. Yu, T. Jiang, J. Wen, *et al*., New insight into the contribution of Ca, Mn, and Mg component to vanadium extraction from vanadium slag, *J. Environ. Chem. Eng.*, 12(2024), No. 5, art. No. 113966.

[29] C.Q. Li, T. Jiang, J. Wen, T.X. Yu, and F.F. Li, Review of leaching, separation and recovery of vanadium from roasted products of vanadium slag, *Hydrometallurgy*, 226(2024), art. No. 106313.

[30] Z.X. Wu and L. Jiang, Study on vanadium precipitation by hydrolysis of chromium–vanadium solution, *Iron Steel Vanadium Titanium*, 41(2020), No. 5, p. 22.

[31] G.J. Gao, Vanadium extraction from vanadium–chromium solution by hydrothermal–hydrolysis precipitation, *Iron Steel Vanadium Titanium*, 38(2017), No. 5, p. 15.

[32] J. Wen, T.X. Yu, T. Jiang, H.Y. Sun, M. Li, and Y. Peng, Effect of chromium content on the phase composition, crystallization and components extraction of vanadium slag, *Process. Saf. Environ. Prot.*, 165(2022), p. 13.

[33] R. Duan. *Preparation of High Purity V_2O_5 and Study on Crystalline Mechanism of Ammonium Vanadate* [Dissertation]. Central South University. Changsha, 2011, p. 12.

[34] S.M. Liao and T.L. Bai, *Foreign Vanadium Metallurgy*, Metallurgy Industry Press, Beijing, 1985, p. 62.

[35] L. Jiang, W.Y. He, G.C. Du, H. Zheng, and Y. Peng, Implication of hydrolysis on vanadium precipitation with acidic ammonium salt from high concentration of alkaline vanadium solution, *Korean J. Chem. Eng.*, 40(2023), No. 10, p. 2513.